NASA TECHNICAL NOTE

NASA TN D-7702

NASA TN D-7702

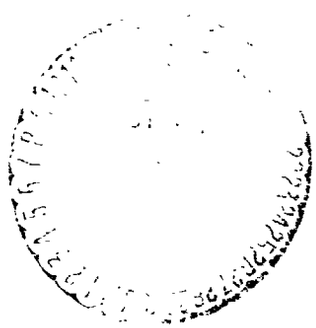

SOME EFFECTS OF TIP FINS ON WING FLUTTER CHARACTERISTICS

by Robert C. Goetz and Robert V. Doggett, Jr.

Langley Research Center
Hampton, Va. 23665

NATIONAL AERONAUTICS AND SPACE ADMINISTRATION •• WASHINGTON, D. C. •• OCTOBER 1974

1. Report No. NASA TN D-7702	2. Government Accession No.	3. Recipient's Catalog No.
4. Title and Subtitle SOME EFFECTS OF TIP FINS ON WING FLUTTER CHARACTERISTICS		5. Report Date October 1974 6. Performing Organization Code
7. Author(s) Robert C. Goetz and Robert V. Doggett, Jr.		8. Performing Organization Report No. L-9644
9. Performing Organization Name and Address NASA Langley Research Center Hampton, Va. 23665		10. Work Unit No. 502-32-02-08 11. Contract or Grant No.
12. Sponsoring Agency Name and Address National Aeronautics and Space Administration Washington, D.C. 20546		13. Type of Report and Period Covered Technical Note 14. Sponsoring Agency Code
15 Supplementary Notes		

16. Abstract

A wind-tunnel investigation has been conducted over the Mach number range from about 0.6 to 1.2 to determine the effects of large tip fins on the flutter characteristics of a swept wing. The basic wing configuration had an aspect ratio of 0.95, leading-edge sweep of 40°, and trailing-edge sweep of 21°. Two of these configurations were modified with tip fins of 60° dihedral and had effective aspect ratios of 1.5 and 2.2. In general, the results indicate that the addition of tip fins reduces the flutter speed, with the larger fin having the greater effect.

Comparison of the experimental flutter speeds at Mach numbers between 0.60 and 0.90 with calculated values obtained by using doublet-lattice unsteady aerodynamic theory was good. Analytical results where structural and aerodynamic effects of the tip fins were isolated indicated that the reduction in flutter speed produced by the addition of the fins was caused by both effects, with the structural effect being the more pronounced.

17. Key Words (Suggested by Author(s))
Flutter
Transonic speeds
Nonplanar surfaces

18. Distribution Statement
Unclassified – Unlimited

STAR Category 32

19. Security Classif. (of this report)	20. Security Classif. (of this page)	21. No. of Pages	22. Price*
Unclassified	Unclassified	31	$3.25

*For sale by the National Technical Information Service, Springfield, Virginia 22151

SOME EFFECTS OF TIP FINS ON WING FLUTTER CHARACTERISTICS

By Robert C. Goetz and Robert V. Doggett, Jr.
Langley Research Center

SUMMARY

A wind-tunnel investigation has been conducted over the Mach number range from about 0.6 to 1.2 to determine the effects of large tip fins on the flutter characteristics of a swept wing. The basic wing configuration had an aspect ratio of 0.95, leading-edge sweep of 40°, and trailing-edge sweep of 21°. Two of these configurations were modified with tip fins of 60° dihedral and had effective aspect ratios of 1.5 and 2.2. In general, the results indicate that the addition of tip fins reduces the flutter speed, with the larger fin having the greater effect.

Comparison of the experimental flutter speeds at Mach numbers between 0.60 and 0.90 with calculated values obtained by using doublet-lattice unsteady aerodynamic theory was good. Analytical results where structural and aerodynamic effects of the tip fins were isolated indicated that the reduction in flutter speed produced by the addition of the fins was caused by both effects, with the structural effect being the more pronounced.

INTRODUCTION

For the vehicle designs emerging for space transportation systems, it is evident that interactive effects from both a steady and unsteady aerodynamic viewpoint are becoming more significant. These vehicle designs are combinations of multiple bodies and lifting surfaces; the latter are dictated by requirements for the maneuverability and the stability and control during the ascent, reentry, gliding, and landing phases of flight. Lifting-surface concepts that appear attractive for satisfying these requirements may have the feature of nonplanar intersecting surface segments. One such concept is a swept wing with large tip fins.

Wings with large tip fins are a concern to the aeroelastician since their structural design might be significantly influenced by flutter clearance requirements. For example, if the mass of the tip fin is not negligible in relation to that of the wing alone, the flutter speed is modified by its presence. Whereas a change in mass distribution is known to have a large effect on the flutter speed, the associated change in aerodynamic forces may also be a significant factor.

Concern over designs where aerodynamic interference may be important to flutter is not new. When T-tail designs began to emerge in the early 1950's, it was quickly recognized that a better understanding of aerodynamic interference was needed to determine the flutter characteristics of these aerodynamically complex designs. This need resulted in the development of unsteady aerodynamic theories applicable to T-tails such as those presented in references 1 and 2. In addition to analytical studies some experimental T-tail flutter results are available. (For example, see refs. 3 and 4.) Another area that has received attention is tandem-mounted wing—horizontal-tail configurations. Several wind-tunnel-model flutter studies have been conducted on wing-tail configurations, and some results are presented in references 5 and 6. Unsteady aerodynamic theories have been developed for application to wing-tail configurations. A kernel-function procedure is presented in reference 7, and the doublet-lattice method is described in reference 8. Some experimental flutter results are compared in reference 6 with analytical results obtained by using both kernel-function and doublet-lattice unsteady aerodynamic methods. Additional comparisons between experimental and analytical results are presented in reference 9. However, a search of the available literature indicated that there are no published flutter results in the range from high subsonic to low supersonic speeds for wings with large tip fins.

Accordingly, the present investigation was undertaken to determine the importance of the aerodynamic interference effects on the flutter characteristics of a swept wing having a tip fin and to compare experimental and analytical results for subsonic flow obtained from application of the doublet-lattice method.

The experimental program was conducted by using simple semispan models in the Langley 26-inch transonic tunnel over the Mach number range from about 0.6 to 1.2. Three model configurations were tested. The basic wing-alone configuration had an aspect ratio of 0.95, leading-edge sweep of 40°, and trailing-edge sweep of 21°. The other two model configurations had the same leading- and trailing-edge sweep angles, but tip fins with 60° of dihedral (with no toe-in) were added so that the resulting models had effective aspect ratios of 1.5 and 2.2. All model configurations had 10-percent-thick NACA 64-series airfoil sections and were tested at zero angle of attack. A coupled-mode flutter analysis based on doublet-lattice unsteady aerodynamics was performed for Mach numbers of 0.60, 0.80, and 0.90 by using calculated mode shapes and measured frequencies; the results of this analysis are compared with measured results.

SYMBOLS

b_r reference semichord, m

f frequency, Hz

f_f flutter frequency, Hz

f_2 frequency of second natural mode, Hz

g structural damping coefficient

M Mach number

m mass, kg

q dynamic pressure, $\frac{1}{2}\rho V^2$, $kN/m^2 = kPa$

V velocity, meters/second

V_I flutter-speed index parameter, $\frac{V}{b_r \omega_2 \sqrt{\mu}}$

v reference volume, m^3

μ mass-ratio parameter, $\frac{m}{\rho v}$

ρ density, kg/m^3

ω_2 reference circular frequency, $2\pi f_2$, rad/sec

Subscripts:

c calculated

e experimental

MODELS

Description

The basic model configuration (wing alone) used in this investigation was a semi-span, aspect-ratio-0.95 wing with no dihedral and having leading-edge sweep of 40° and trailing-edge sweep of 21°. Two other models, consisting of the basic configuration with two different lengths of wing-tip extensions added at a dihedral angle of 60°, were tested in an effort to determine the effects of a tip fin on the flutter characteristics of the basic wing. The fins had the same leading- and trailing-edge sweep as the basic wing and were

oriented at zero angle of attack with respect to the free-stream flow. The two fin models, referred to hereafter as the full-fin and half-fin models, had effective aspect ratios of 2.2 and 1.5, respectively. The effective aspect ratio is defined as the square of the semispan normalized by the total wing area after the fin has been rotated into the plane of the wing. Both the wing and the fins had 10-percent-thick NACA 64-series airfoil sections parallel to the flow. The fins were relatively large compared with the wing; for the full-fin model the fin planform area was about half that of the basic wing, and for the half-fin model the fin planform area was slightly less than one-third that of the basic wing.

Figure 1 is a photograph illustrating the three model configurations. A sketch giving the geometric properties of the models is presented in figure 2.

The models were of simple sandwich construction, consisting of a 0.2235-cm-thick aluminum-alloy core to which balsa wood was bonded with the grain oriented perpendicular to the core. The balsa wood was machined to give the desired NACA 64A010 airfoil shape. The aluminum-alloy core of the model was also used to support the model in a cantilever fashion along the forward two-thirds of the model root. Resistance-type strain gages were mounted on the model core to measure model dynamic response.

Physical Properties and Vibration Characteristics

The total measured mass, natural frequencies f, and structural damping g of the models are given in table I. The natural frequencies, node lines, and still-air damping coefficients of the first four natural structural modes were determined for all three models. The natural frequency for the full-fin-model fifth mode was also determined. The calculated and measured frequencies and nodal patterns are shown in figure 3. These experimental data were obtained by exciting the models at resonance with an interrupter air-jet shaker using the 1g sand technique. For these tests the models were attached to a massive backstop. The mounting arrangement was essentially the same as that used for mounting the models in the wind tunnel. The damping data were obtained from the decaying oscillation that resulted when the pulsating air jet from the shaker was abruptly cut off. The calculated modal data were obtained by using the NASA Structural Analysis (NASTRAN) Computer Program. NASTRAN is described in detail in references 10 and 11. Quadrilateral structural finite elements (NASTRAN QUAD2) were used to model the structure for the calculations. Thirty-six elements were used for the wing portion of all three models; 24 elements were used for the half-tip-fin portion; and 60 elements were used for the full-tip-fin portion. The arrangement of the quadrilateral elements is shown in figure 4. A comparison of the calculated and measured node lines (see fig. 3) indicates fairly good agreement. Although all the frequencies agree reasonably well, ordinarily the best agreement would have been expected for the basic wing

model since this is the simplest structural configuration. However, better agreement was obtained for the two models with tip fins which are structurally more complex than the wing model. The best frequency agreement was obtained for the full-fin model. Although no specific explanation is available, it should be pointed out that some uncertainty was introduced into the analytical model since it was necessary to estimate the stiffness properties of the balsa wood and of the adhesive used to attach the balsa-wood covering to the aluminum-alloy core. The stiffness properties of the aluminum were known, but it was necessary to estimate the properties of the balsa wood and the adhesive by use of typical values of similar material. The estimated values of Young's modulus used for the balsa wood and for the adhesive were 2.83 GPa and 3.45 GPa, respectively. The adhesive was assumed to be 0.056 cm thick.

FLUTTER EXPERIMENTS

Wind Tunnel

The investigation was conducted in the Langley 26-inch transonic tunnel over the Mach number range from about 0.6 to 1.2. This transonic blowdown tunnel has an octagonal test section which measures 66 cm across the flats and has a slot in each corner. The tunnel is capable of operation at stagnation pressures up to about 517 kPa. During operation of the tunnel, the area of the orifice (second minimum) is preset at a given value; as the stagnation pressure, and thus the density, is increased, the test-section Mach number increases until the orifice becomes choked. Thereafter, as the stagnation pressure is further increased, the Mach number remains approximately constant. However, the area of the orifice may also be varied during a test run as the stagnation pressure is increased, or held constant, so that various operating paths of Mach number and density may be followed. Both methods of operation were used in the present investigation.

Test Procedure

The models tested were mounted at midheight on a 7.6-cm-diameter fuselage sting (see fig. 5) which extended forward into the low-speed region of the tunnel. This arrangement prevented the formation of shock waves from the sting nose which might reflect from the tunnel walls onto the models. The sting provided a rigid mount for the models since the mass of the support system was very large compared with the mass of a model. The fundamental frequency of the support system was about 6 Hz, well below the first natural frequency of any of the models.

An optical system displayed an image of the model on a ground-glass screen during the wind-tunnel tests. When flutter was observed visually, the airflow was quickly

stopped in an effort to save the model from being damaged so that it could be utilized in subsequent tests. Before each test run, with the model mounted in the tunnel, frequencies and damping coefficients for the first two natural modes were measured to be certain that the model had experienced no structural damage. The tunnel stagnation pressure, stagnation temperature, test-section static pressure, and model strain-gage signals were continuously recorded on a direct readout recorder. Visual records of the model motion were obtained through the use of two high-speed motion-picture cameras.

FLUTTER ANALYSIS

Subsonic flutter calculations were made for all three models over the Mach number range from 0.60 to 0.90. The flutter equations in matrix notation were expressed in terms of generalized modal coordinates, and the traditional V-g method of solution was used. The calculated natural mode shapes were used in conjunction with the corresponding measured natural frequencies.

Flutter characteristics for all three models were determined by using doublet-lattice unsteady aerodynamic theory. The doublet-lattice unsteady aerodynamic forces were determined by using the method described in references 12 and 13. The doublet-lattice method requires that the lifting surface be subdivided into trapezoidal boxes arranged in streamwise columns. The arrangement of boxes used is shown in figure 6. The same arrangement was used for the wing portion of all three models. There were 50 boxes on the wing, 35 boxes on the half fin, and 50 boxes on the full fin. The two fins shown in the figure have been rotated down into the plane of the paper so that the view is normal to these surfaces. For the doublet-lattice method, a line of acceleration potential doublets is placed at the one-quarter-chord station of each box. An aerodynamic influence coefficient matrix is generated which relates the force on the boxes to the downwash on the boxes. The force acts at the one-quarter-chord point, and the downwash point where the geometrical boundary condition of tangential flow is satisfied is at the three-quarter-chord station. Both the force and downwash points are located at the box midspan station. The aerodynamic influence coefficient is used in conjunction with the mode shapes to determine a generalized aerodynamic force matrix.

Subsonic lifting-surface theory (kernel function) was also used to calculate the flutter characteristics of the basic wing model at a Mach number of 0.80. The technique used to generate the kernel-function unsteady aerodynamic forces was based on that described in reference 14. For the kernel-function method, a linear integral equation which relates the pressure distribution to the downwash at selected control points on the lifting surface is solved numerically for the unsteady pressure distribution. The downwash at the control points is a function of the structural mode shapes used in the analysis. The kernel-function method generates directly a generalized unsteady aerodynamic

force matrix. Thirty-six control points were used in the kernel-function analysis. The locations of these points are indicated by the circular symbols in figure 6.

Since the aerodynamic models for the doublet-lattice and kernel-function methods were different from the structural model (compare figs. 4 and 6), it was necessary to interpolate the modal deformations determined at the structural grid points to the modal displacements and streamwise slopes required at the aerodynamic points. This transformation was accomplished by using the surface spline function described in reference 15. Since the surface spline function is based on the small deflection equation of an infinite plate, it is very good for interpolating structural mode shapes. In interpolating the modes for the two models with tip fins, two spline functions were used. One spline function was generated by using the modal displacements on the wing portion, and the second was generated by using the modal displacements on the fin portion. The modal deformations along the juncture between the wing and fin portions were included in the generation of both splines to assure continuity in the interpolation.

The V-g method of flutter solution requires many solutions of a complex eigenvalue problem with the reduced frequency as a parameter and is relatively expensive in terms of computer costs. Since one of the most costly processes is the determination of the generalized unsteady aerodynamic forces, it has become more or less standard practice to calculate the generalized aerodynamic forces for a relatively small number of values of the reduced frequency parameter and to interpolate these forces for their values at a larger number of reduced frequencies. Interpolated aerodynamic forces were used to obtain the calculated flutter results presented in this paper. A natural cubic spline was used to perform the interpolation. A discussion of the use of cubic spline functions for aerodynamic force interpolation is presented in reference 16. For the doublet-lattice calculations, the aerodynamic forces were calculated at 6 values of reduced frequency and interpolated to 50 values of reduced frequency. For the kernel function, there were 20 calculated values and 400 interpolated values.

RESULTS AND DISCUSSION

The basic experimental flutter results are presented in table II and figure 7. The data presented in the figure include the variations with Mach number of the mass-ratio parameter μ, of the flutter-frequency ratio f_f/f_2, and of the flutter-speed index parameter V_I. The flutter-speed-index-parameter curves represent stability boundaries, with the stable region (no flutter) below the curve. This parameter depends on the physical properties of the model, in particular the stiffness, and the atmosphere in which it operates. When plotted as the ordinate against Mach number, curves of constant dynamic pressure are lines parallel to the Mach number abscissa. The mass-ratio parameter μ is defined as the ratio of the mass of the model to the mass of a representative

surrounding volume of test medium. The volume used in this study is that contained in the conical frustum having base diameters equal to the respective model root and tip chords and a height equal to the sum of the individual spans of the wing and tip fin portions where the span of the fin is measured in the plane of the fin. These volumes for the wing, half-fin, and full-fin models were 2061.9 cm^3, 2504.5 cm^3, and 2740.6 cm^3, respectively. The second natural frequency f_2 was used as the reference frequency. The same reference length b_r was used for all three models. This length of 6.26 cm was the semichord at the three-quarter-span station of the wing portion of the models.

No unusual trends are shown by the data presented in figure 7 for the half-fin and full-fin models. The flutter boundary is similar to that usually observed, namely, a more or less constant value at subsonic speeds followed by a decrease in flutter-speed index at transonic Mach numbers with a sharp increase in flutter-speed index as the flow becomes supersonic. No experimental flutter results were obtained for the basic wing model. This model did not flutter within the available operating range of the wind tunnel. At transonic speeds this model was tested at dynamic pressure levels of about 140 kPa which is considerably above the flutter boundary determined for the other two models.

In terms of the flutter-speed index parameter, a comparison of the flutter boundary for the half-fin model (fig. 7(a)) with that of the full-fin model (fig. 7(b)) would lead the reader to believe that the full-fin configuration is less susceptible to flutter. This is not the true situation, however, since the full-fin model fluttered at lower dynamic pressures than did the half-fin model over the Mach number range of the study. Normally the flutter-speed index parameter V_I is successful in correlating flutter data between similar configurations; however, this was not true for the wing-tip configurations for this study. The variation of flutter dynamic pressure with Mach number for both of these models is presented in figure 8. Both sets of data show the same trend, namely, a more or less constant value at subsonic speeds, a dramatic decrease in the transonic range, and an increase in value at supersonic speeds. For both models, the transonic minimum dynamic pressure was about 45 percent of the value at Mach 0.6. Although no flutter data were obtained for the basic wing model, it is known that its flutter boundary is considerably above those of the models with fins. As mentioned previously, the wing model was tested at transonic Mach numbers to a dynamic pressure of 140 kPa. Therefore, it can be concluded that the addition of the fins to the basic wing has a significant adverse effect on the flutter characteristics. Further, the larger the fin, the greater is the decrease in flutter speed.

Experimental and analytical flutter boundaries for the two models with tip fins are compared in figure 9. The data are presented as the variation with Mach number of the flutter-frequency ratio and the flutter-speed index parameter. The experimental curves

shown are the faired curves from figure 7. Additional analytical flutter results, including basic wing model data, are presented in table III. The calculated results in the figure were obtained by using a four-mode analysis with doublet-lattice unsteady aerodynamic forces and the densities corresponding to the experimental values. One calculation was made at M = 0.80 (see table III(c)) for the full-fin model by using five natural modes in the analysis. Since this result was almost the same as the four-mode result, it was assumed that the use of four modes was sufficient to insure convergence of the flutter solution. Also, some calculated flutter results were obtained by using densities different from the experimental values to assess the sensitivity of the calculated flutter speeds to mass-ratio effects. Although the calculated flutter speeds did indicate a sensitivity of flutter speed to changes in density, no large effect was observed over the range of the study. In general, the calculated flutter results predict higher flutter frequencies and speeds than were found experimentally. However, the agreement between the two sets of data is considered to be good and shows that the doublet-lattice unsteady aerodynamic theory can be used with some confidence in predicting the flutter speeds of wings with large tip fins.

As has been observed, there was a marked reduction in the flutter speed when a tip fin was added to the basic wing model. This effect could be caused by both structural and aerodynamic effects. An analytical study was made to separate the aerodynamic and structural effects, and the results of this study are shown in figure 10. The data are presented in the form of the variation of flutter dynamic pressure with Mach number for the wing model, the full-fin model with no aerodynamic forces acting on the fin portion, and the full-fin model with aerodynamic forces acting on the fin. Additional calculated flutter results for all three cases are presented in table III. All results presented in the figure were obtained by using the doublet-lattice unsteady aerodynamic theory with the exception of a M = 0.80 result obtained by using kernel-function aerodynamics for the wing model. It is interesting to note that the kernel-function and doublet-lattice results are almost the same. The calculated full-fin model results are the same as those presented in figure 9(b). Flutter characteristics for the full-fin model without aerodynamic forces on the fin (hereafter referred to as full fin without aerodynamics) were calculated by using a five-mode analysis and the densities corresponding to the full-fin model experiment. A check calculation at M = 0.80 using only four modes for this configuration gave the same result as was obtained by using five modes. (See table III(d).) Consequently, it can be assumed that the flutter solutions using five modes for the full fin without aerodynamics case have converged. The basic-wing-model results presented in the figure were obtained by using four modes and an air density of 2.701 kg/m^3. For both the basic wing model and the full fin without aerodynamics case, additional calculations were made with density as a variable to determine whether any significant mass-ratio effects were present. (See tables III(a) and III(d).) No significant mass-ratio effects

were noted over the density range covered. An examination of the data in figure 10 (compare upper and lower curves) indicates that there is a very large decrease in the flutter dynamic pressure with the addition of the full fin to the basic wing model. For example, at $M = 0.60$ this reduction is 77 percent and includes both aerodynamic and structural effects. By removing the aerodynamic forces from the full fin, it is possible to determine what proportion of the reduction in flutter dynamic pressure is due to the structural changes which occur when the fin is added to the wing. The flutter boundary without fin aerodynamic forces is shown as the middle curve in the figure. This flutter boundary is substantially lower than the basic wing boundary. At $M = 0.60$ the flutter dynamic pressure is reduced by 63 percent. The results in figure 10 indicate that for the configuration studied in this investigation, the greatest proportion of the reduction in flutter dynamic pressure was due to the structural and inertial changes produced by the addition of the tip fin. However, although the aerodynamic effects were smaller than the structural effects, they were not insignificant. The aerodynamic effect was responsible for about 20 percent of the total decrease in flutter dynamic pressure. It should be noted that the relative proportion of structural and aerodynamic effects of tip fins on wing flutter characteristics would differ for other configurations.

CONCLUDING REMARKS

The effects of the addition of two different tip fins to a basic wing have been determined experimentally over the Mach number range from about 0.6 to 1.2. The basic wing had an aspect ratio of 0.95, a leading-edge sweep of 40°, and a trailing-edge sweep of 21°. Both the small and large tip fins had a dihedral of 60° and, in terms of surface area, were one-third and one-half as large as the basic wing, respectively. The results indicate that the addition of the tip fins reduces the flutter speed, with the larger fin having the greater effect. No unusual behavior was noted in the variation of the flutter speed with Mach number for the models with tip fins.

Comparison of the experimental flutter boundaries at subsonic speeds with calculated results obtained by using doublet-lattice unsteady aerodynamic theory was good. The results of an analytical study where structural and aerodynamic effects of the tip fins were isolated indicated that the reduction in flutter speed produced by the addition of the fins was caused by a combination of structural and aerodynamic effects, with the structural effect being the more pronounced.

Langley Research Center,
National Aeronautics and Space Administration,
Hampton, Va., August 12, 1974.

REFERENCES

1. Stark, Valter J. E.: Aerodynamic Forces on a Combination of a Wing and a Fin Oscillating in Subsonic Flow. SAAB TN 54, Saab Aircraft Co. (Linköping, Sweden), Feb. 1964.

2. Davies, D. E.: Generalized Aerodynamic Forces on a T-Tail Oscillating Harmonically in Subsonic Flow. R. & M. No. 3422, Brit. A.R.C., 1966.

3. Stahle, C. V.: Transonic Effects on T-Tail Flutter. RM-24, The Martin Co., Feb. 1959.

4. Ruhlin, Charles L.; Sandford, Maynard C.; and Yates, E. Carson, Jr.: Wind-Tunnel Flutter Studies of the Sweptback T-Tail of a Large Multijet Cargo Airplane at Mach Numbers to 0.90. NASA TN D-2179, 1964.

5. Topp, L. J.; Rowe, W. S.; and Shattuck, A. W.: Aeroelastic Considerations in the Design of Variable Sweep Aeroplanes. Aerospace Proceedings 1966, Vol. 2, Joan Bradbrooke, Joan Bruce, and Robert R. Dexter, eds., Macmillan and Co., Ltd., c.1967, pp. 851-870.

6. Mykytow, W. J.; Noll, T. E.; Huttsell, L. J.; and Shirk, M. H.: Investigations Concerning the Coupled Wing-Fuselage-Tail Flutter Phenomenon. J. Aircraft, vol. 9, no. 1, Jan. 1972, pp. 48-54.

7. Laschka, Boris; and Schmid, Heinrich: Unsteady Aerodynamic Forces on Coplanar Lifting Surfaces in Subsonic Flow (Wing – Horizontal Tail Interference). Jahrb. 1967 WGLR, Hermann Blenk and Werner Schulz, eds., c.1968, pp. 211-222.

8. Albano, Edward; and Rodden, William P.: A Doublet-Lattice Method for Calculating Lift Distributions on Oscillating Surfaces in Subsonic Flows. AIAA J., vol. 7, no. 2, Feb. 1969, pp. 279-285.

9. Mykytow, W. J.; Olsen, J. J.; and Pollock, S. J.: Application of AFFDL Unsteady Load Prediction Methods to Interfering Surfaces. Symposium on Unsteady Aerodynamics for Aeroelastic Analyses on Interfering Surfaces, Pt. II, AGARD-CP-80-71, Apr. 1971.

10. MacNeal, Richard H., ed.: The NASTRAN Theoretical Manual. NASA SP-221, 1970.

11. McCormick, Caleb W., ed.: The NASTRAN User's Manual. NASA SP-222, 1970.

12. Giesing, J. P.; Kalman, T. P., and Rodden, W. P.: Subsonic Unsteady Aerodynamics for General Configurations. Part I, Vol I – Direct Application of the Nonplanar Doublet-Lattice Method. AFFDL-TR-71-5, Pt. I, Vol I, U.S. Air Force, Nov. 1971.

13. Giesing, J. P.; Kalman, T. P.; and Rodden, W. P.: Subsonic Unsteady Aerodynamics for General Configurations. Part I, Vol II – Computer Program H7WC. AFFDL-TR-71-5, Pt. I, Vol II, U.S. Air Force, Nov. 1971.

14. Watkins, Charles E.; Woolston, Donald S.; and Cunningham, Herbert J.: A Systematic Kernel Function Procedure for Determining Aerodynamic Forces on Oscillating or Steady Finite Wings at Subsonic Speeds. NASA TR R-48, 1959.

15. Harder, Robert L.; and Desmarais, Robert N.: Interpolation Using Surface Splines. J. Aircraft, vol. 9, no. 2, Feb. 1972, pp. 189-191.

16. Desmarais, Robert N.; and Bennett, Robert M.: An Automated Procedure for Computing Flutter Eigenvalues. J. Aircraft, vol. 11, no. 2, Feb. 1974, pp. 75-80.

TABLE I.- MEASURED MODEL PHYSICAL PROPERTIES

Model	Mass, kg			Mode 1		Mode 2		Mode 3		Mode 4		Mode 5	
	Wing portion	Fin portion	Total	f, Hz	g	f, Hz	g	f, Hz	g	f, Hz	g	f, Hz	g
Basic wing	0.19579	------	0.19579	76.2	0.0100	270.	0.0188	490.	0.020	766	(a)	(a)	(a)
Half fin	.19579	0.06201	.25780	40.6	.0167	169.2	.0223	217.	.0260	533	(a)	(a)	(a)
Full fin	.19579	.10058	.29637	29.2	.0163	96.6	.020	121.4	.0244	350	(a)	575	(a)

[a]Not measured.

TABLE II.- EXPERIMENTAL FLUTTER RESULTS

(a) Half-fin model

M	V, m/s	ρ, kg/m^3	q, kPa	μ	$\sqrt{\mu}$	V_I	f_f, Hz	f_f/f_2
0.607	190.2	5.231	94.62	19.68	4.44	0.644	77.8	0.460
.720	228.6	3.695	96.55	27.86	5.28	.651	76.4	.452
.790	252.4	2.824	89.94	36.45	6.04	.628	75.3	.445
.818	233.2	3.386	92.05	30.40	5.51	.635	74.4	.440
.899	253.9	3.067	98.84	33.57	5.79	.658	72.8	.430
.910	285.3	1.273	51.81	80.86	8.99	.477	51.0	.301
.916	287.7	1.062	43.95	96.96	9.85	.439	49.5	.293
.913	294.4	1.845	79.98	55.79	7.47	.592	70.0	.414
.917	289.0	1.098	45.83	93.77	9.68	.448	51.0	.301
.920	281.3	1.747	69.14	58.92	7.68	.551	52.0	.307
.922	289.0	1.871	78..	55.02	7.42	.585	61.0	.361
.945	297.2	1.149	50.75	89.56	9.46	.472	49.7	.294
.959	297.5	1.005	44.47	102.43	10.12	.442	49.0	.290
.966	302.4	1.041	47.59	98.88	9.94	.457	47.5	.281
1.047	313.9	1.386	68.32	74.25	8.62	.547	55.8	.330

TABLE II.- EXPERIMENTAL FLUTTER RESULTS – Concluded

(b) Full-fin model

M	V, m/s	ρ, kg/m^3	q, kPa	μ	$\sqrt{\mu}$	V_I	f_f, Hz	f_f/f_2
0.598	188.7	2.670	47.52	40.51	6.36	0.780	58.0	0.600
.647	209.4	1.902	41.69	56.86	7.54	.731	48.1	.498
.690	223.7	1.840	46.05	58.78	7.67	.768	51.4	.532
.730	236.8	1.484	41.63	72.86	8.54	.730	44.3	.459
.773	251.8	1.273	40.34	84.95	9.22	.719	46.4	.480
.784	254.2	1.118	36.13	96.70	9.83	.680	44.0	.455
.787	254.8	1.237	40.16	87.43	9.35	.717	46.0	.476
.794	254.8	1.304	42.33	82.94	9.11	.736	53.3	.552
.799	259.4	1.154	38.84	93.67	9.68	.705	49.5	.512
.810	260.0	1.227	41.46	88.16	9.39	.729	51.0	.528
.817	261.5	1.170	40.01	92.44	9.61	.716	50.5	.523
.818	263.0	1.093	37.80	98.98	9.95	.696	52.1	.539
.844	270.7	1.077	39.45	100.40	10.02	.711	46.4	.480
.847	271.9	1.077	39.81	100.40	10.02	.714	44.4	.460
.852	273.7	1.031	38.61	104.91	10.24	.703	4[illegible].4	.480
.855	274.0	1.062	39.86	101.86	10.09	.714	'8.7	.504
.860	274.9	1.057	39.93	102.36	10.12	.715	54.8	.567
.891	280.4	.959	37.69	112.81	10.62	.695	42.6	.441
.895	278.9	.861	33.47	125.65	11.21	.655	40.0	.414
.910	28[illegible].5	.634	26.02	170.59	13.06	.577	33.1	.343
.922	290.5	.531	22.39	203.72	14.27	.536	31.2	.323
.971	305.7	.521	24.32	207.75	14.41	.558	32.3	.334
.993	313.0	.644	31.56	167.86	12.96	.636	38.7	.401
1.030	321.0	.995	51.23	108.72	10.43	.810	47.4	.491
1.190	341.4	1.325	77.18	81.65	9.04	.994	57.3	.593

TABLE III.- CALCULATED FLUTTER RESULTS

(a) Basic wing model

M	V, m/s	ρ, kg/m^3	q, kPa	μ	$\sqrt{\mu}$	V_I	f_f, Hz	f_f/f_2	Method	Number of modes
0.600	413.0	2.701	230.32	35.16	5.93	0.656	188.2	0.697	Doublet lattice	4
.800	411.5	2.701	228.63	35.16	5.93	.653	167.9	.622	↓	↓
.900	397.5	2.701	213.38	35.16	5.93	.631	150.6	.558		
.800	600.0	1.226	220.58	77.48	8.80	.642	157.8	.584	Kernel function	4
.800	561.2	1.415	222.83	67.10	8.19	.645	156.5	.580	↓	↓
.800	524.5	1.627	223.76	58.38	7.64	.646	158.7	.588		
.800	491.2	1.862	224.56	51.01	7.14	.647	158.7	.588		
.800	467.5	2.062	225.25	46.06	6.79	.648	159.0	.589		
.800	419.6	2.577	226.87	36.85	6.07	.651	159.3	.590		
.800	410.9	2.701	227.95	35.16	5.93	.652	159.4	.590		
.800	384.6	3.092	228.66	30.71	5.54	.653	159.5	.591		
.800	357.3	3.608	230.23	26.32	5.13	.656	159.8	.592		

(b) Half-fin model

M	V, m/s	ρ, kg/m^3	q, kPa	μ	$\sqrt{\mu}$	V_I	f_f, Hz	f_f/f_2	Method	Number of modes
0.600	281.9	2.824	112.25	36.45	6.04	0.702	107.1	0.633	Doublet lattice	4
.600	212.5	5.231	118.08	19.68	4.44	.720	109.0	.644	Doublet lattice	4
.800	271.8	2.824	104.31	36.45	6.04	.676	92.0	.544	Doublet lattice	4
.900	368.5	1.273	86.42	80.86	8.99	.616	79.3	.469	↓	↓
.900	251.5	2.824	89.29	36.45	6.04	.626	78.8	.466		
.900	192.7	5.231	97.09	19.68	4.44	.653	82.2	.486		

TABLE III.- CALCULATED FLUTTER RESULTS – Concluded

(c) Full-fin model

M	V, m/s	ρ, kg/m^3	q, kPa	μ	$\sqrt{\mu}$	V_I	f_f, Hz	f_f/f_2	Method	Number of modes
0.600	199.4	2.670	53.07	40.51	6.36	0.824	73.8	0.764	Doublet lattice	4
.800	322.5	.861	47.57	125.65	11.21	.781	64.1	.664	Doublet lattice	4
.800	304.3	1.031	47.72	104.91	10.24	.782	64.3	.666	↓	↓
.800	278.5	1.237	47.97	87.43	9.35	.784	64.1	.664		
.800	277.9	1.237	47.75	87.43	9.35	.782	64.6	.669		
.800	238.0	1.716	48.61	63.01	7.94	.789	64.5	.668		
.800	196.4	2.577	49.72	41.97	6.48	.798	65.5	.678		
.900	304.8	.861	39.98	125.65	11.21	.716	56.1	.581	Doublet lattice	4

(d) Full-fin model with no aerodynamic forces on fin portion

M	V, m/s	ρ, kg/m^3	q, kPa	μ	$\sqrt{\mu}$	V_I	f_f, Hz	f_f/f_2	Method	Number of modes
0.600	446.0	0.861	85.61	125.65	11.21	1.047	114.5	1.185	Doublet lattice	5
.600	250.0	2.673	83.56	40.45	6.36	1.034	114.7	1.187	Doublet lattice	5
.800	436.5	.861	81.98	125.65	11.21	1.025	114.2	1.182	Doublet lattice	4
.800	436.8	.861	82.10	125.65	11.21	1.025	114.2	1.183	↓	5
.800	362.6	1.237	81.31	87.43	9.35	1.020	114.3	1.183		5
.900	425.7	.861	77.99	125.65	11.21	.999	114.0	1.180	Doublet lattice	5

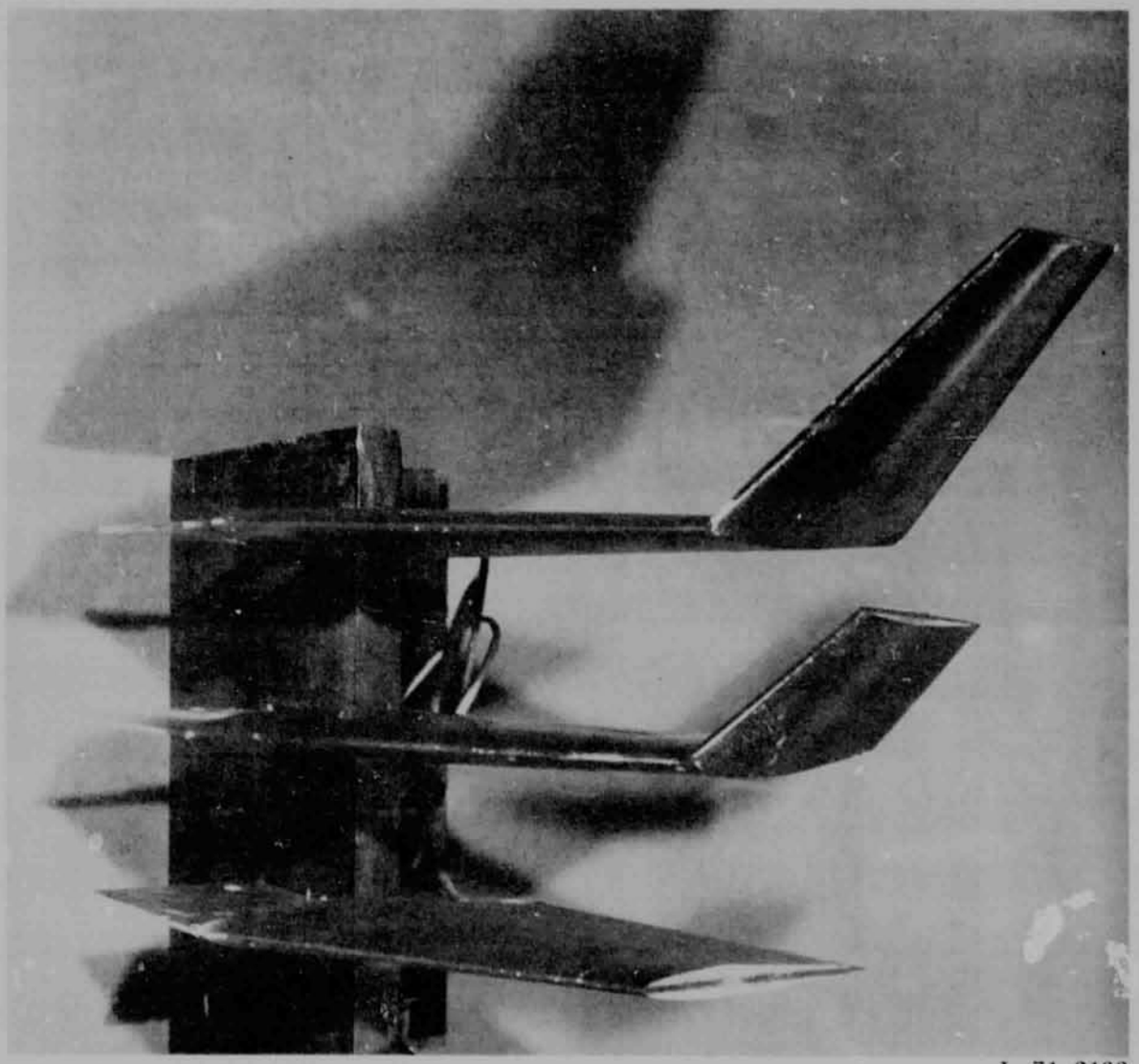

L-71-2133

Figure 1.- Model configurations.

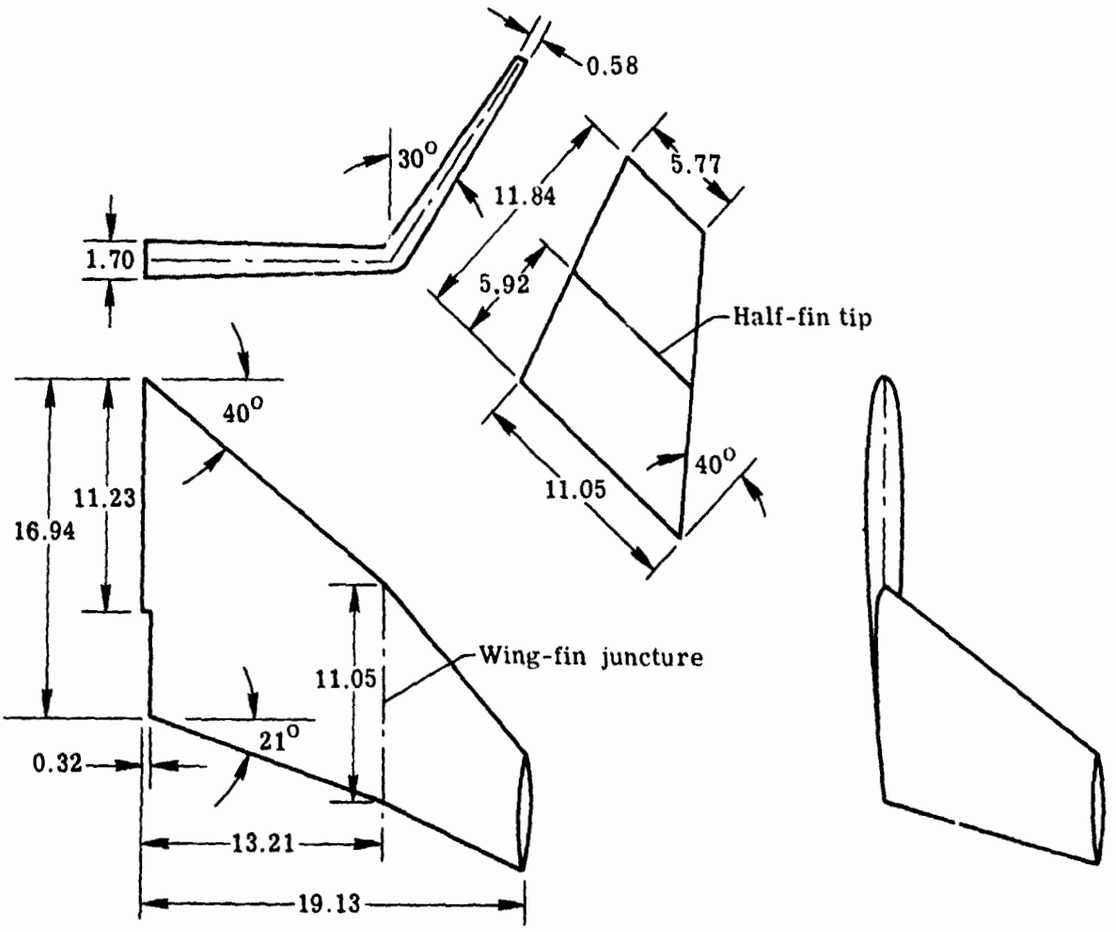

Figure 2.- Model geometric properties. All dimensions are in centimeters.

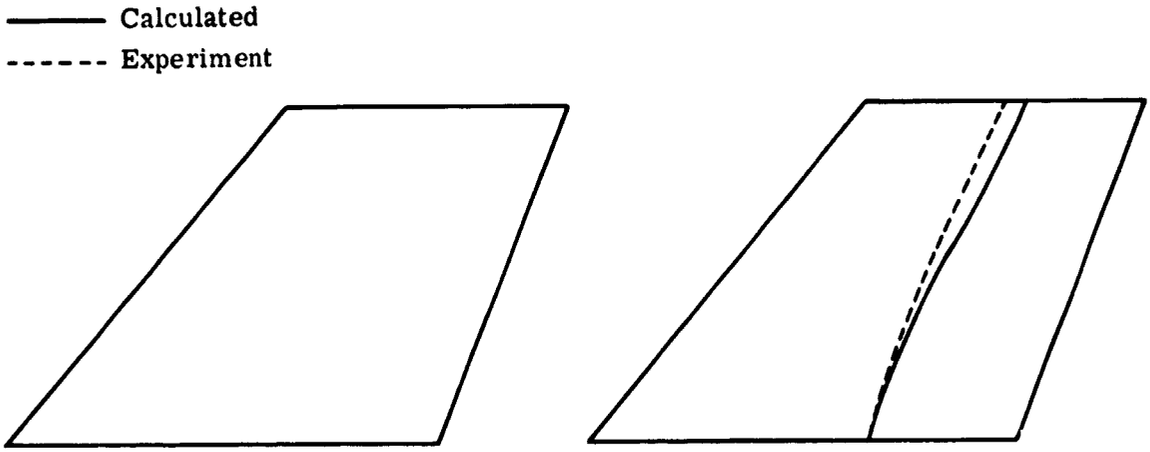

Mode 1: f_e = 76.2 Hz, f_c = 85.7 Hz

Mode 2: f_e = 270 Hz, f_c = 251.2 Hz

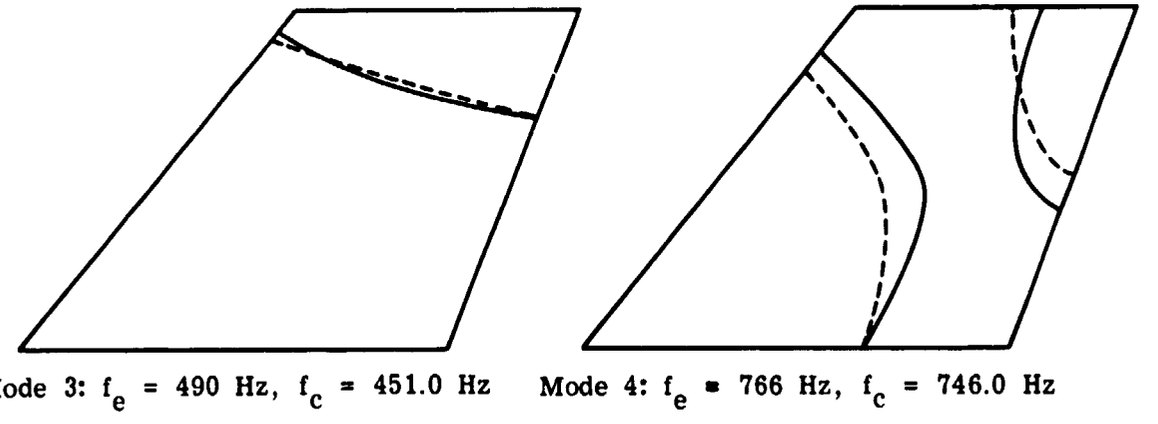

Mode 3: f_e = 490 Hz, f_c = 451.0 Hz

Mode 4: f_e = 766 Hz, f_c = 746.0 Hz

(a) Basic wing model.

Figure 3.- Measured and calculated node lines and natural frequencies.

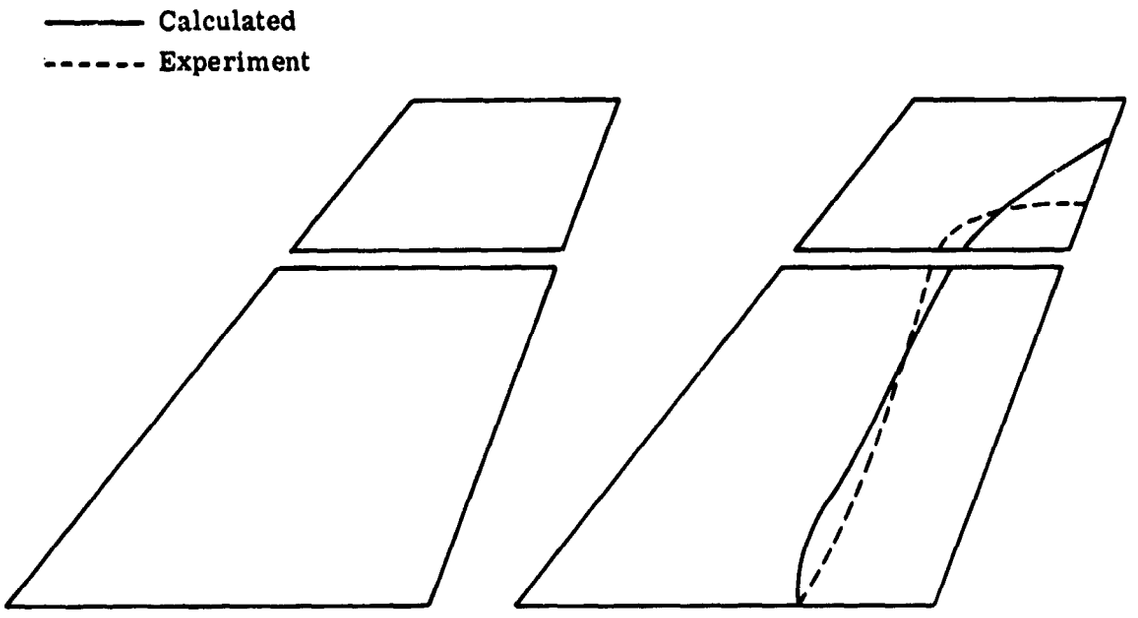

Mode 1: f_e = 40.6 Hz, f_c = 45.7 Hz Mode 2: f_e = 169.2 Hz, f_c = 170.9 Hz

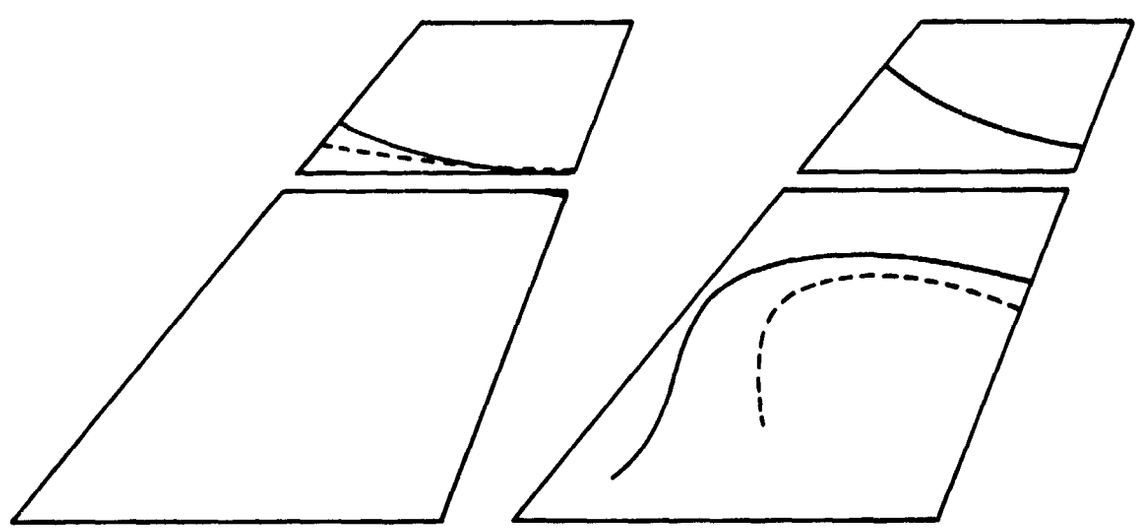

Mode 3: f_e = 217 Hz, f_c = 219.6 Hz Mode 4: f_e = 533 Hz, f_c = 514.0 Hz

(b) Half-fin model.

Figure 3.- Continued.

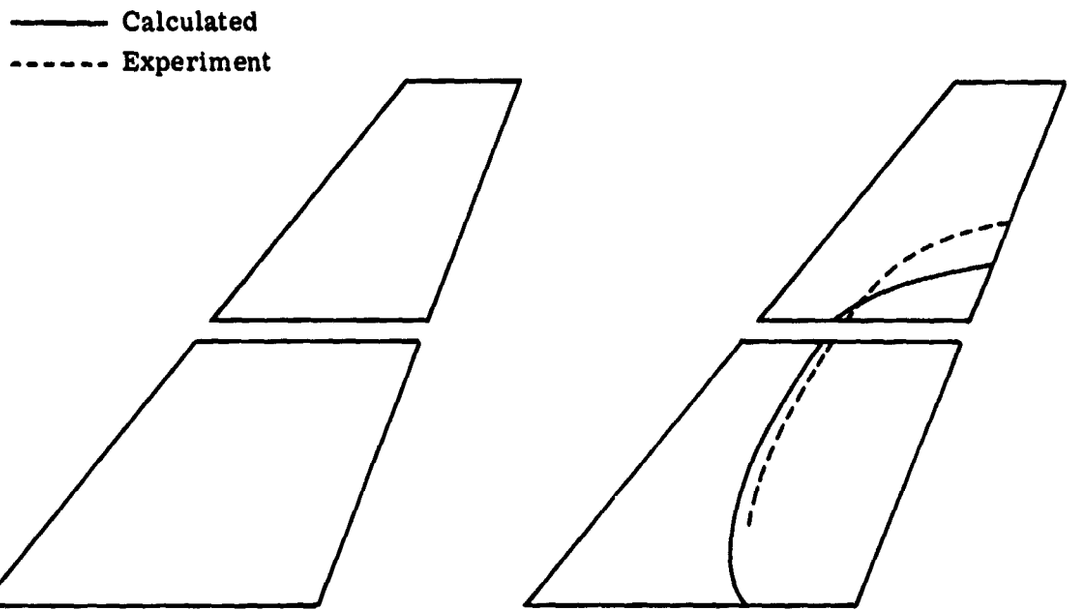

Mode 1: f_e = 29.2 Hz, f_c = 31.4 Hz Mode 2: f_e = 96.6 Hz, f_c = 94.0 Hz

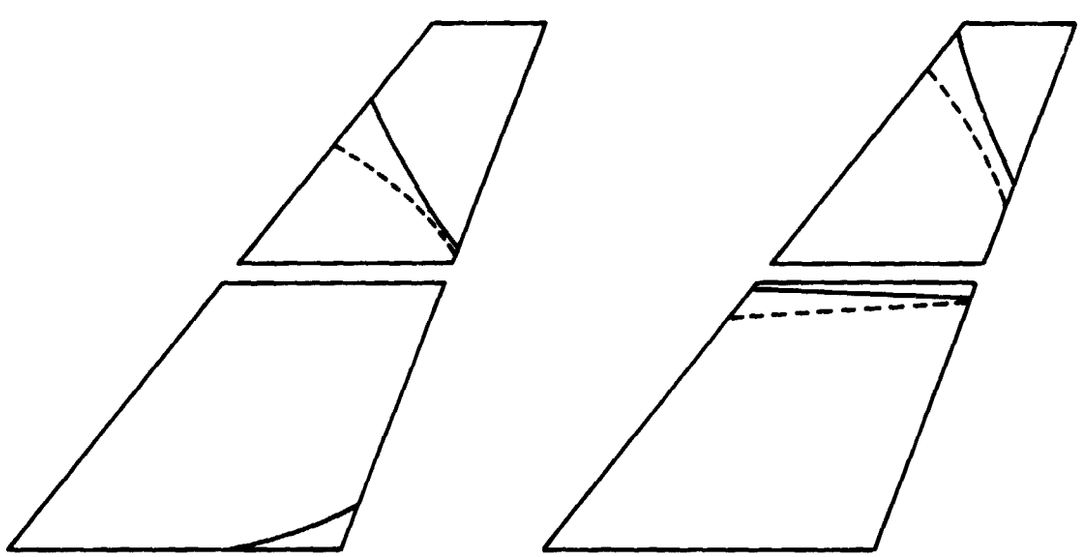

Mode 3: f_e = 121.4 Hz, f_c = 127.0 Hz Mode 4: f_e = 350 Hz, f_c = 338.1 Hz

(c) Full-fin model.

Figure 3.- Concluded.

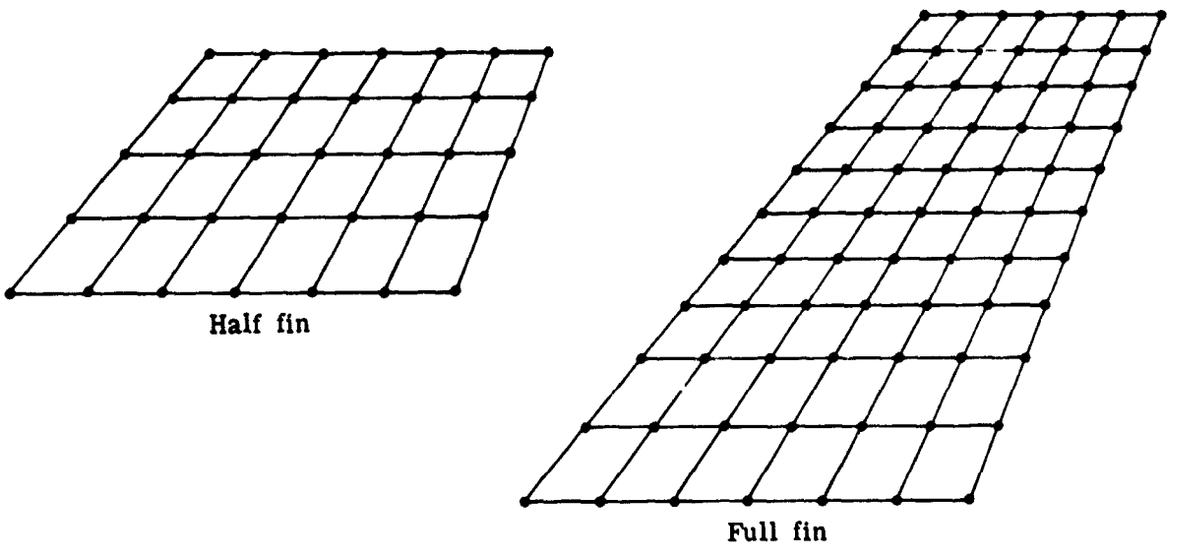

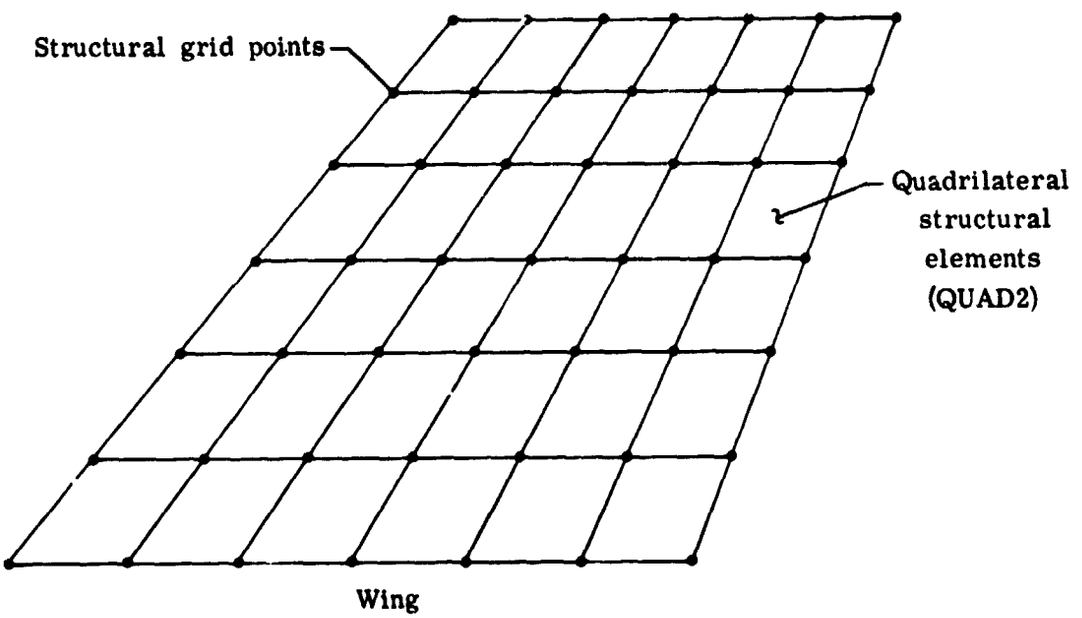

Figure 4.- NASTRAN structural model.

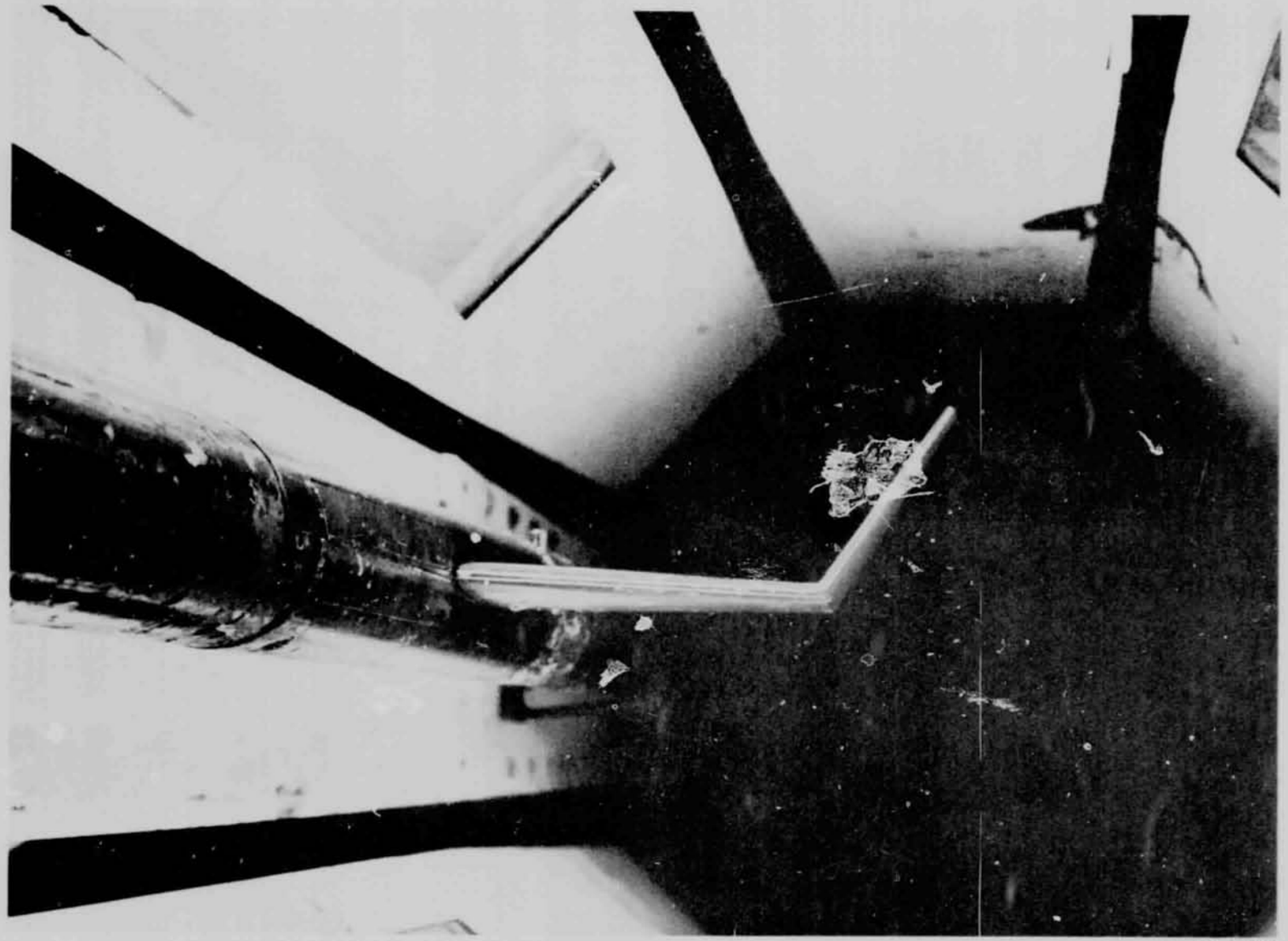

L-71-2136

Figure 5. - Full-fin model mounted in wind tunnel.

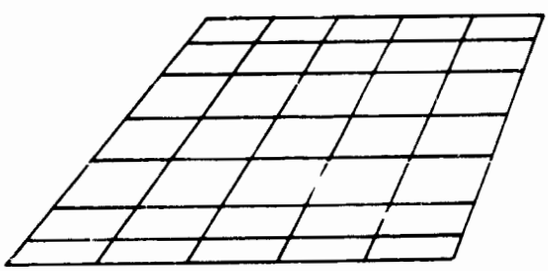

Half fin

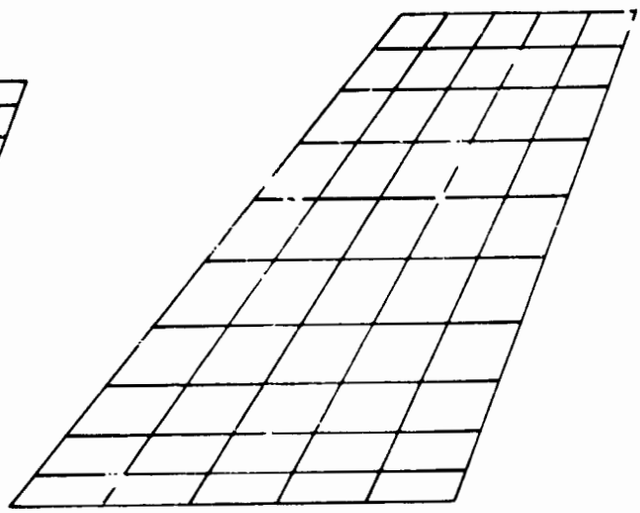

Full fin

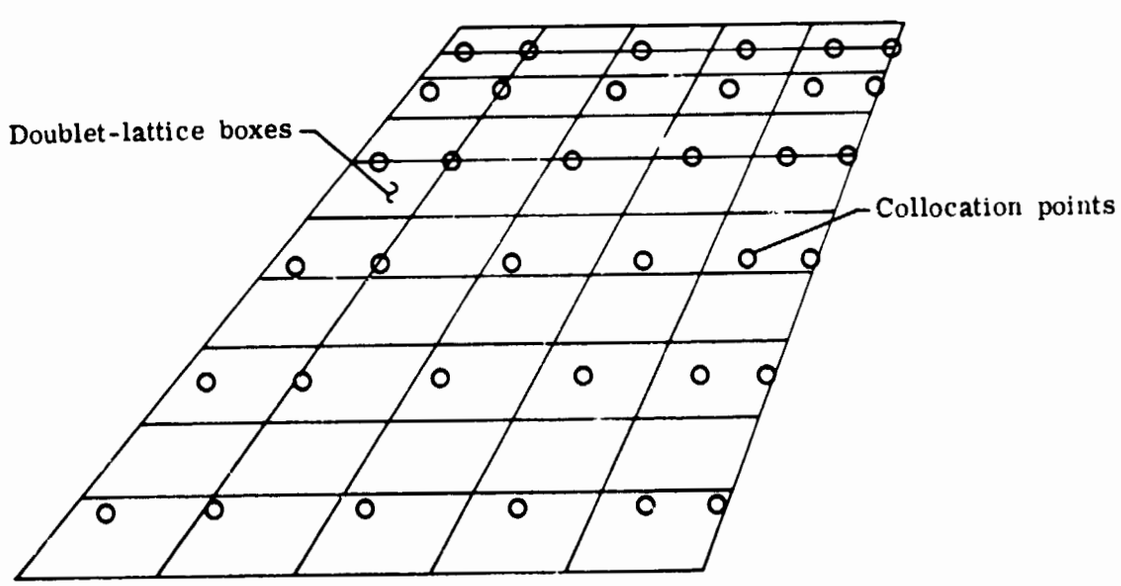

Wing

Figure 6.- Aerodynamic model.

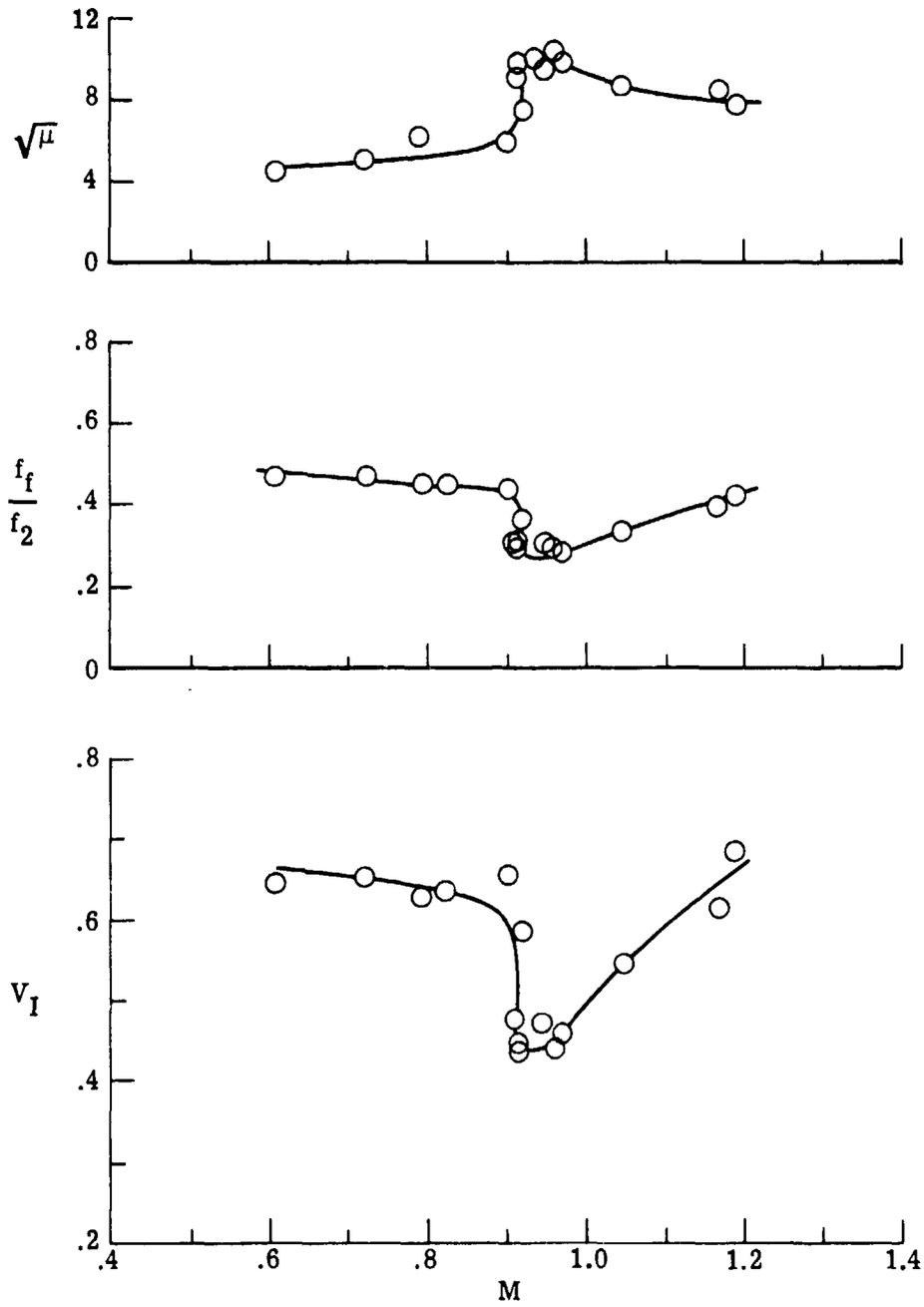

(a) Half-fin model.

Figure 7.- Experimental flutter results.

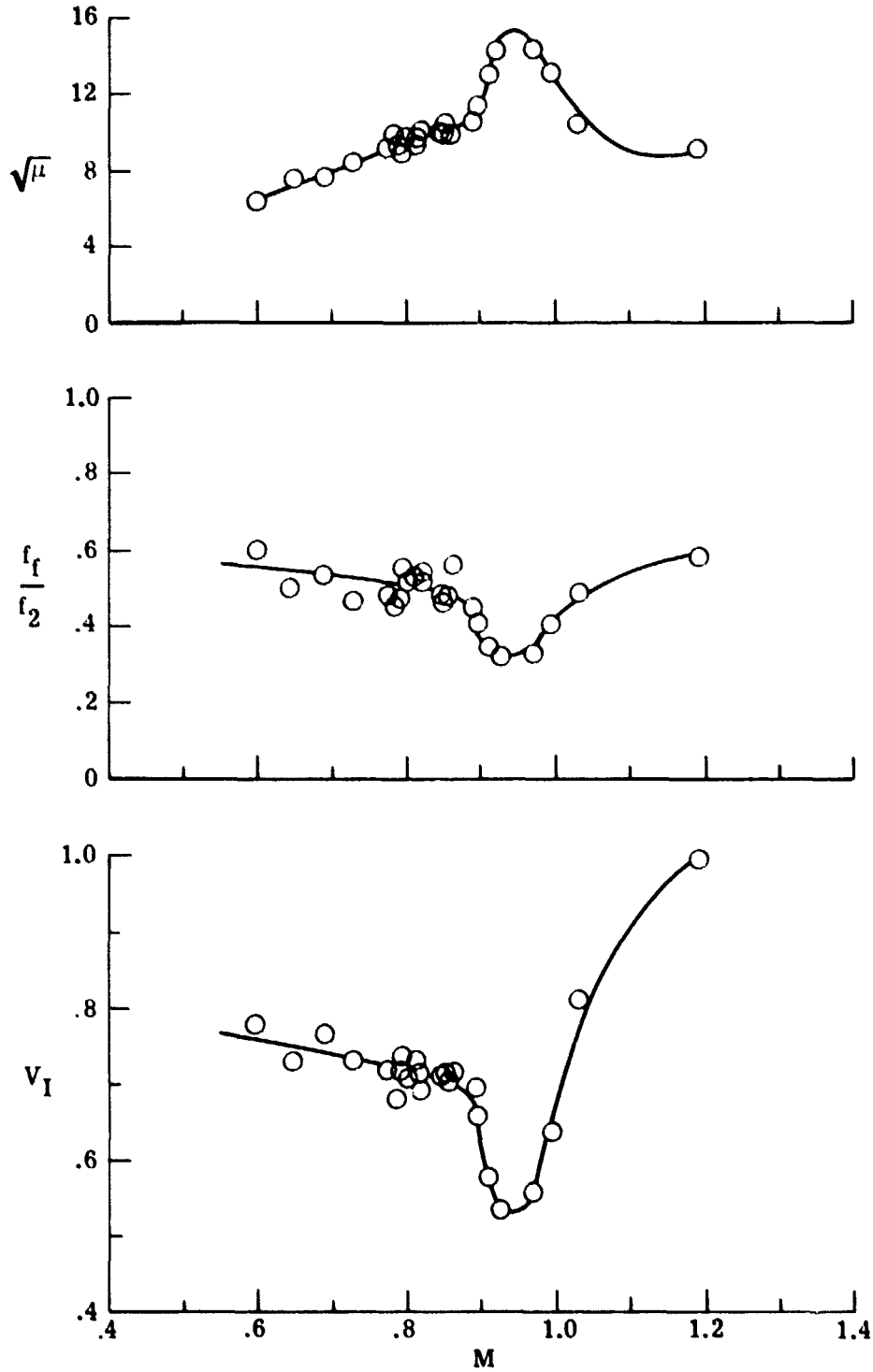

(b) Full-fin model.

Figure 7.- Concluded.

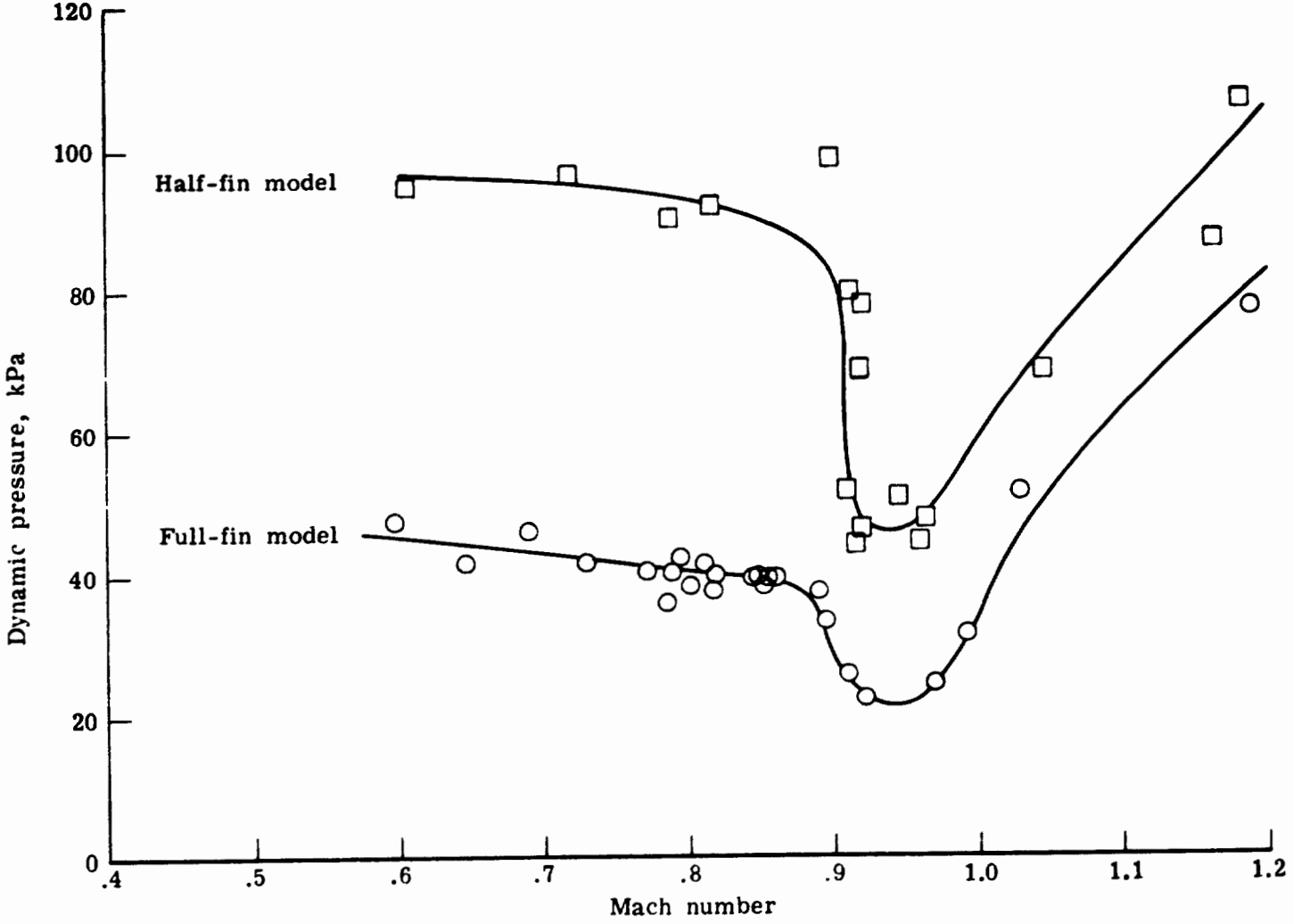

Figure 8.- Variation of flutter dynamic pressure with Mach number.

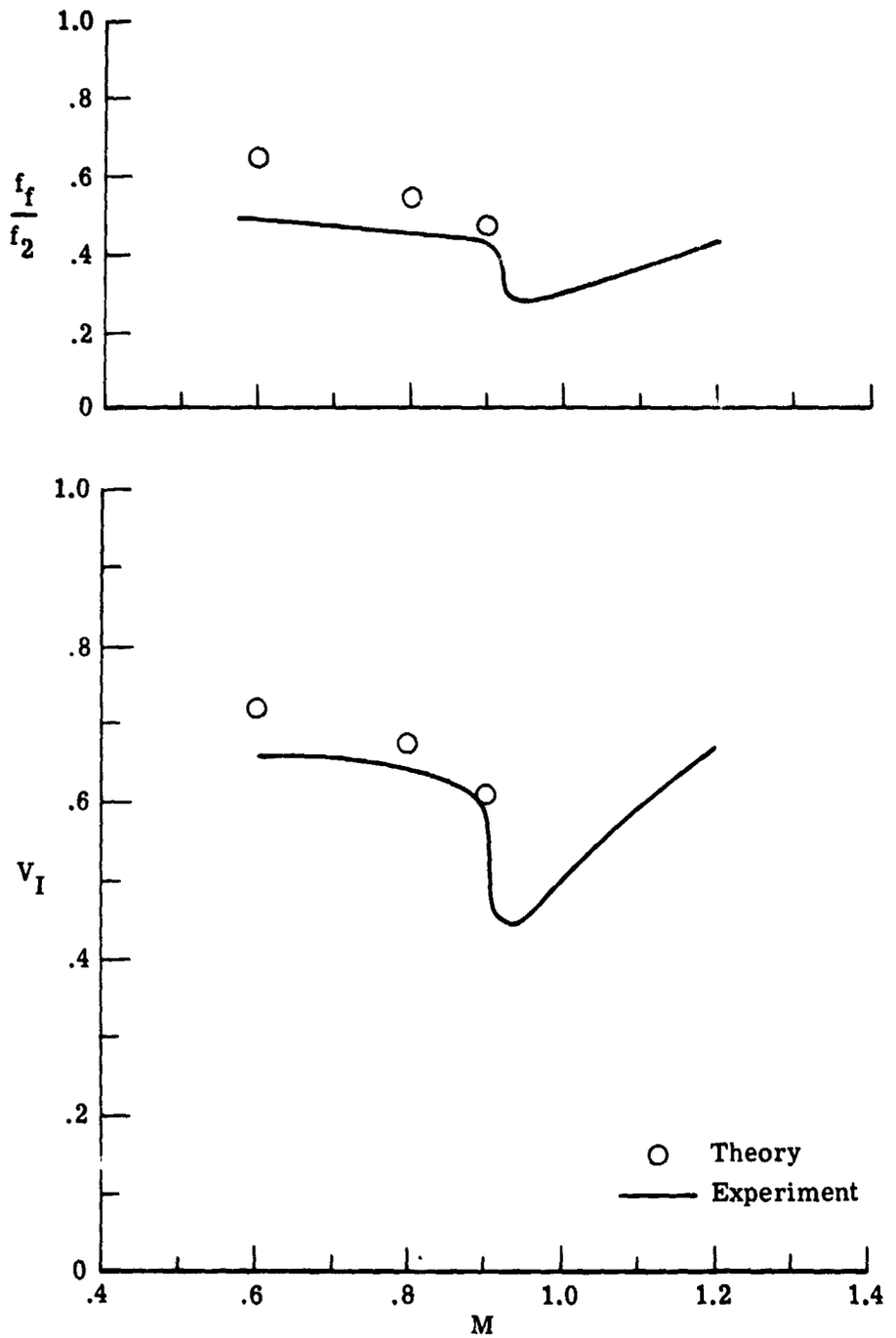

(a) Half-fin model.

Figure 9.- Comparison of calculated and experimental flutter results.

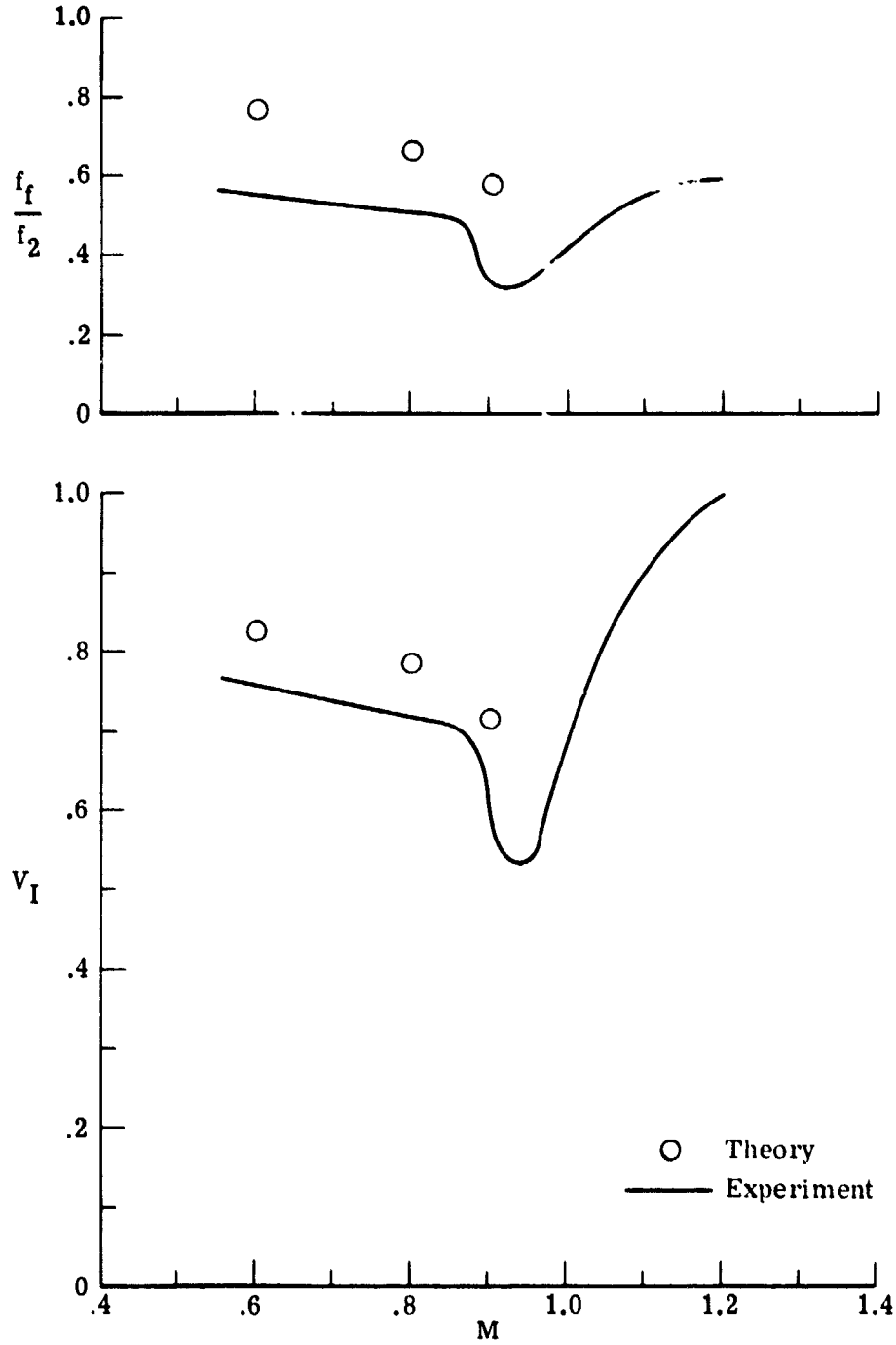

(b) Full-fin model.

Figure 9.- Concluded.

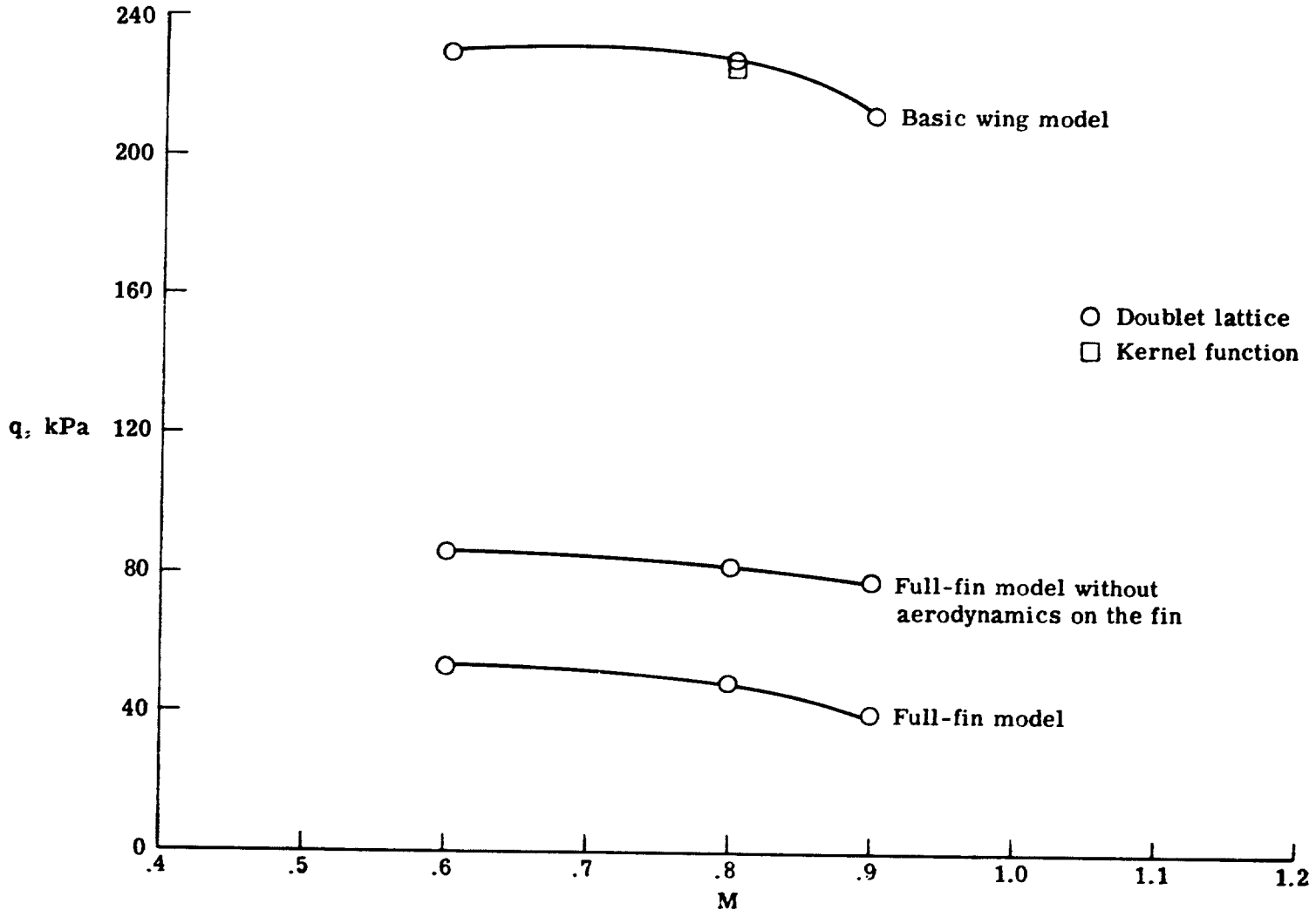

Figure 10.- Calculated effect of tip fin on wing flutter dynamic pressure.